Wavelet-Based Representation of Biological Shapes

Bin Dong*, Yu Mao*, Ivo D. Dinov**, Zhuowen Tu**, Yonggang Shi**, Yalin Wang**, Arthur W. Toga**

* Department of Mathematics, University of California, Los Angeles, CA 90095
** Center for Computational Biology, Laboratory of Neuro Imaging
635 S. Charles Young Dr., #225, University of California, Los Angeles, Los Angeles, CA 90055

Abstract. Modeling, characterization and analysis of biological shape and form are important in many computational biology studies. Shape representation challenges span the spectrum from small scales (e.g., microarray imaging and protein structure) to the macro scale (e.g., neuroimaging of human brains). In this paper, we present a new approach for representation and analysis of biological shape using wavelets. We apply the new technique for multi-spectral shape decomposition and for studying shape variability between populations using brain cortical and subcortical surfaces. The wavelet-space induced shape representation allows us to study the multi-spectral nature of the shape geometry, topology and features. Our results are very promising and compared to the spherical-wavelets method generally provide a shape representation, which is more compact and allows utilization of diverse wavelet bases.

Keywords. wavelets, shape, spherical harmonics, brain imaging, brain mapping.

1 Introduction

1.1 General

Imaging, representation, geometric modeling and topologic characterization of shape and form are important components of Computational Biology. They apply across the vast length scales between genotypes to phenotypes, from the small scale of microarray imaging for genomics, to the larger scale of neuroimaging of human brains. Here we review the existent techniques and algorithms and present a new approach for representation and analysis of biological shape using wavelets. We apply the new method for multi-spectral shape decomposition and for studying shape variability between populations using brain cortical and subcortical surfaces.

1.2 Literature Review

Recently, N. Hacker et al. used conformal mapping and spherical wavelets to analyze biological shapes (see [9, 10]). Their idea is first mapping the original shape onto a unit 2-sphere using a certain conformal mapping so that one obtains a $\mathbb{R}^3$- valued function f defined on the sphere; and then interpolate the function f onto the regular triangular mesh on the sphere (which is generated by recursively subdividing an icosahedron); and then finally, apply spherical wavelet transform to the interpolated function. The spherical wavelets they used were introduced by P. Schröder and W. Sweldens in [15], which were constructed using lifting scheme (see W. Sweldens [14] and F. Arandiga et. al. [1]).

In this paper, we also start from a $\mathbb{R}^3$- valued function f given by a certain mapping from $\mathbb{R}^3$ to S^2. After that, we linearly interpolate the function f onto a triangular mesh, which is generated by recursively subdividing an octahedron in $\mathbb{R}^3$ (not restricted on the sphere) and then transforming the mesh onto the sphere. This method was first introduced by E. Praun and H. Hoppe (see [13]) under the scope of computer graphics. The major advantage of it is that we can transform the subdivided octahedron to a unit square so that we obtain an image with $\mathbb{R}^3$ - valued entries (which were called geometric image in [13]), and then we can apply traditional X-lets (e.g. wavelets, framelets, curvelets etc.) decomposition. In this way we have

plenty of good bases and frames to choose according the application we have. More details of this approach are given in the second part of this paper.

1.3 Brain Mapping Challenges

Understanding the relationship between the structure and function of the human brain in vivo has been the driving motivation for many neurosciences research for centuries. The research efforts not only focus on studying normal development but also understanding alterations in various clinical populations including schizophrenia, Huntington's disease, Alzheimer's disease, Williams Syndrome, autism, stroke, chronic drug abuse, as well as pharmacological interventions. For instance, there are multiple studies underway to quantify the differences between the brain structure of schizophrenic patients and healthy individuals in different stages of this disease. Detection of these significant differences via neuroimaging studies is not only useful to elucidate the link between change in cognitive profile and change in brain structure, but also to improve diagnosis particularly in early stages of the disease. With the increasing interest in carrying out such studies with large numbers of subjects, there is a need for a unified framework for image segmentation to identify the structure of interest (e.g. caudate, ventricles, cerebral cortex, sulcal regions) (see Z. Tu et. al. [24]), and morphometric analysis which requires methods for shape representation, shape comparison, and change in shape measurement (see P. Thompson and A. Toga [20]).

1.4 Outline of the Paper

The rest of the paper is organized as follows. Section 2 gives a detailed explanation of how we manage data, and how we build multiscaled representations for the shapes we have (i.e. hippocampus and cortical surfaces). We provide some experimental results in section 3: multiscaled sparse representation of shapes, curvature-like characterization of shapes using wavelet coefficients, and statistical analysis of healthy and unhealthy hippocampus/cortices. In section 4, we give discussions of the results in section 3 and suggest possible future work.

2 Methods

In this section we describe our test data and the specific approach we took to represent shape using wavelets, as well as the statistical analyses we carry on the wavelet-based shape decomposition to identify group, population, time or variation differences.

2.1 Data

Cortical Models: Surface objects of normal subjects and Williams syndrome patients were used to explore the power of our method to synthesize the energy of the shape content in a few wavelet coefficients. The demographics of the population included age (29.2 9.0), genders (approximately 50/50) and IQ scores, P. Thompson et. al. [21]. Nonbrain tissue (i.e., scalp, orbits) was removed from the images, and each image volume was resliced into a standard orientation who "tagged" 20 standardized anatomical landmarks in each subject's image data set that corresponded to the same 20 anatomical landmarks defined on the ICBM53 average brain (see Mazziotta et al. [12], Thompson et. al. [22]). Automated tissue segmentation was conducted for each volume data set to classify voxels as most representative of gray matter, white matter, CSF, or a background class (representing extracerebral voxels in the image) on the basis of signal intensity. The procedure fits a mixture of Gaussian distributions to the intensities in each image before assigning each voxel to the class with the highest probability, Shattuck et. al. [16]. Then each individual's cortical surface was extracted and three-dimensionally rendered using automated software, MacDonald [11]. Each resulting cortical surface was represented as a high-resolution mesh of 131,072 surface triangles spanning 65,536 surface points.

Hippocampal surfaces: High-resolution MRI scans were acquired from 12 AD patients ages 68.4 ± 1.9 and 14 matched controls 71.4 ± 0.9, each scanned twice, 2.1 ± 0.4 years apart. 3D parametric mesh models of the left and right hippocampi and temporal horns were manually, Thompson et. al. [23]. For each scan, a radio frequency bias field correction algorithm eliminated intensity drifts due to scanner field inhomogeneity, using a histogram spline sharpening method, Sled et. al. [19]. Images were then normalized

by transforming them to ICBM53 stereotaxic space, Evens et. al. [6], with automated image registration software, Collins et. al. [3]. To equalize image intensities across subjects, registered scans were histogram-equalized.

Each 3D surface is mapped to a unit sphere in $\mathbb{R}^3$ with 1-to-1 correspondence. For cortical surfaces, the conformal mapping method of Shi et. al. [17, 18] is used for hippocampal surfaces and that of Gu et. al. [8]

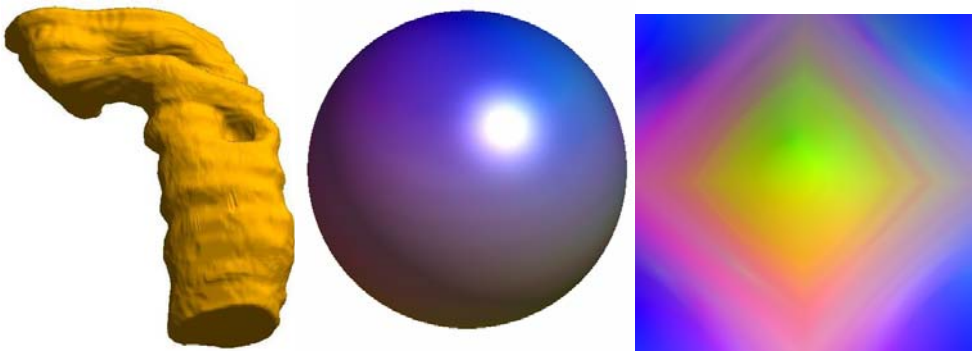

(a) (b) (c)

Fig. 1. Figure (a) is the shape we chose; (b) is the spherical function visualized as a spherical colored image; (c) is the geometric image.

for cortical surfaces. For hippocampal surfaces, harmonic maps to the sphere are computed under the constraints of a set of automatically detected landmark curves (see [17, 18]).

2.2 Wavelet-Based Representation of Shapes

From section 2.1, we got a function defined on the unit sphere S^2, which has vector values in $\mathbb{R}^3$. However, the values of the function were only given on an irregular grid on the sphere. To apply the wavelet transform, we need to get the value of the function on a much more regular spherical grid. There are many approaches to get such kind of grids. The construction of the spherical mesh grid, sometimes called spherical triangular map, is an interesting subject itself (see e.g. Buss and Fillmore [2], and Praun

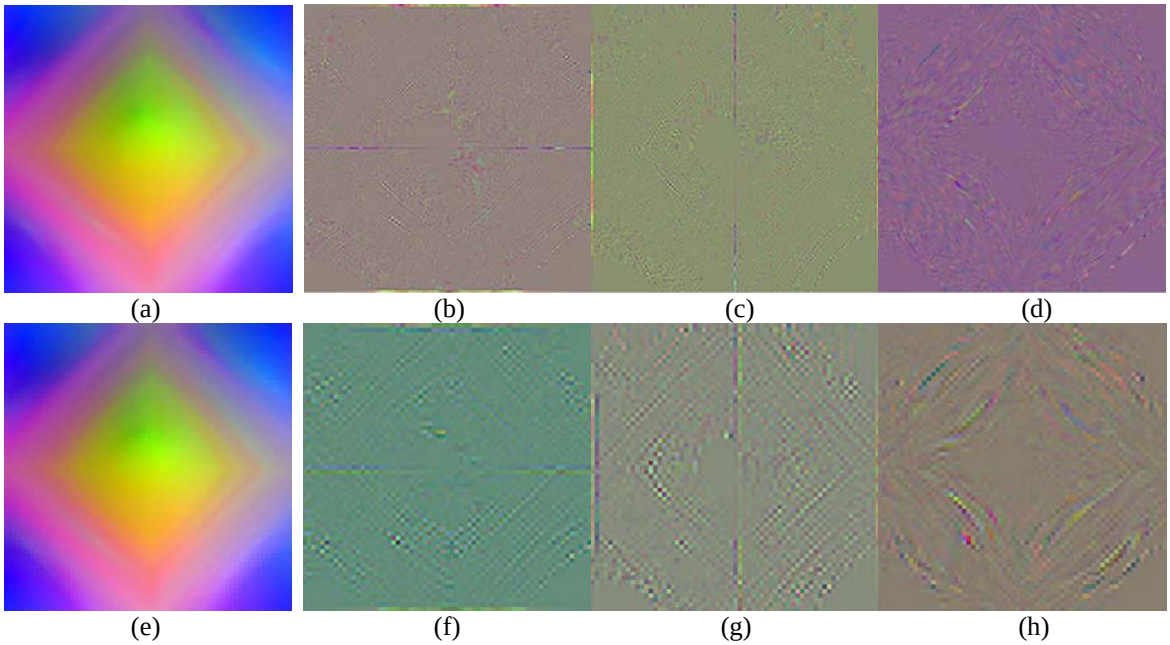

(a) (b) (c) (d)

(e) (f) (g) (h)

Fig. 2. Two-levels wavelet decomposition: (a) and (e) are the low frequency coefficients of level one and two; (b)-(d) are wavelet coefficients of level 1 and band 1-3; (f)-(h) are wavelet coefficients of level 2 and band 1-3.

and Hoppe [13]). The basic idea is to start from a polyhedral base, which gives a simple but perfect grid on sphere, and then use some appropriate scheme to subdivide the mesh. A comparison of such techniques can be found in [13].

In our approach, we start from a recursive subdivision of the octahedral base. By mapping the subdivision grid onto the unit sphere, we get a regular grid structure on the sphere, and the function values on such a spherical grid can be obtained by linear interpolation. The reason we choose octahedron is that it can be unfolded to a plain image easily. Therefore, we can build a 1-1 map between a sphere and an image without too much distortion, and the data of a shape is transformed to a $\mathbb{R}^3$- valued function defined on a plain image, which gives a geometric image (as shown in Figure 1).

Since the mesh on the plain image is nothing but a Cartesian grid, a huge family of X-lets can be used to analyze properties of the geometric image. The wavelets that we shall use in the following experiments are Daubechies' Biorthogonal Wavelets [4]. We note that the boundary condition is a little complicated in this case. Topological saying, the two halves of each side of the image must be identified with each other. Thus, we need to setup corresponding boundary rules for the wavelet filters.

Figure 2 shows how the decomposition is carried out to the geometric image we have. Since all low frequency and wavelet coefficients has x, y, and z three components, all coefficients are visualized as color images.

2.3 Multiscaled curvature-like characterization

As shown in Figure 2 above, for each level and band of the wavelet coefficients, we have x, y, and z three components. The coefficient vectors reflect details of the shape at each position and scale. Indeed, the wavelet vectors can be treated as the displacement between the observed position and the predicted position calculated from the convolution of the wavelet filter and the scale coefficients of the neighboring vertices. Therefore, the direction of the wavelet vector gives us some information of the local geometric properties. For example, if we consider the wavelet vector at a local sunken area, then the approximated position interpolated from the neighboring vertices should be outer than the observed vertex, which means that the wavelet vector is pointing outwards.

However, we cannot tell the geometric property of the shape from the wavelet coefficients directly, and a single wavelet coefficient itself is geometrically meaningless, so we combine the three components by calculating the inner product of the wavelet vector and the normal vector of the shape. As what we explained above, these inner products reflect geometric property at the corresponding position. In this way, a so called multiscaled curvature-like characterization of the shape is obtained: For given scale (or level), we compute normal of the shape at all positions under that scale and take the inner product of the normal with the wavelet coefficient vector. We then obtain a set of curvature-like coefficients within each level and band. The statistical analysis given in Section 3.2 is based on this representation. Figure 3 shows how this representation can be used to find cortical sulci and gyri.

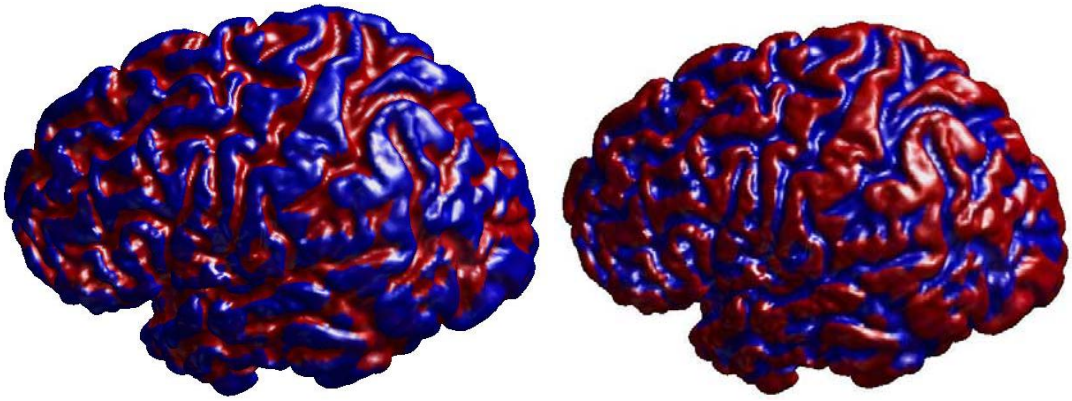

(a) (b)

Fig. 3. Red regions in figure (a) and (b) are the sulcal and girial regions of a given cortex respectively.

3 Results

3.1 Multiscaled Sparse Representation

One of the most important properties of traditional wavelet transform is that it gives a multiscaled representation of the underlying function and the representation is sparse. We now show that our method as discussed in the previous section also gives a multiscaled sparse representation for the biological shapes we have. Figure 4 and 5 shows the multiscaled representation provided by the wavelet transform, and Figure 6 and 7 shows the sparcity of the representation, where one can see that even with only 2500 coefficients, the reconstructed shapes preserve most of the features of the original shapes.

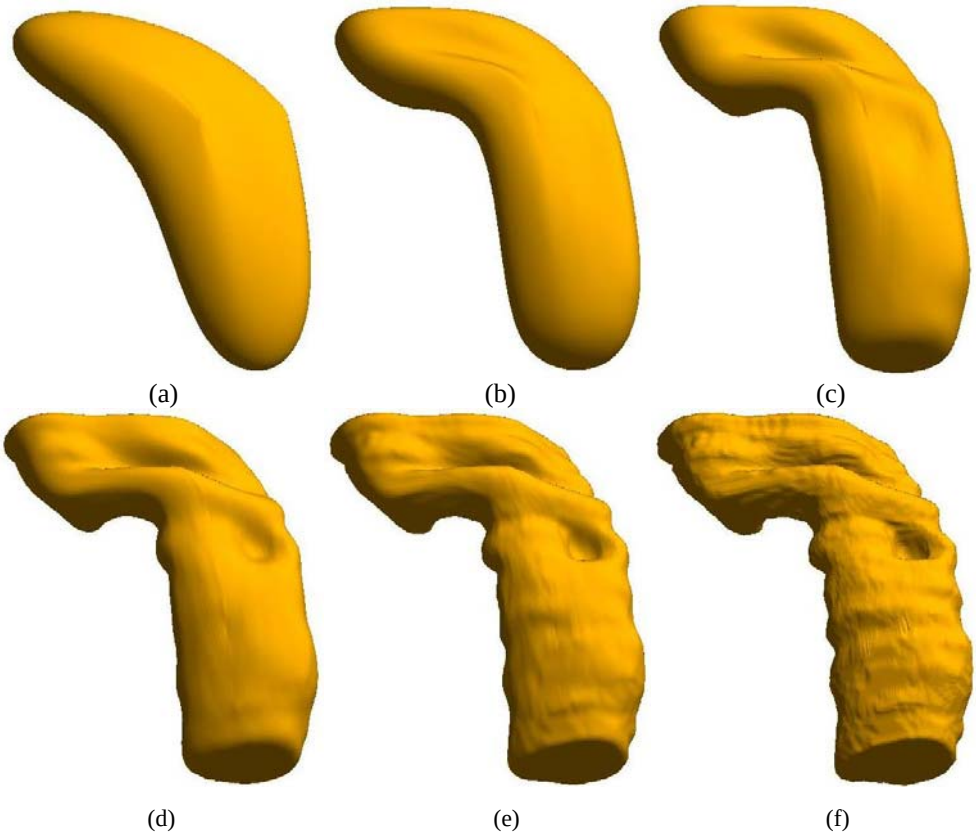

Fig. 4. Figures (a)-(e) present a multiscaled representation of the hippocampus from courser approximation to finer approximation. Figure (f) is the original hippocampus.

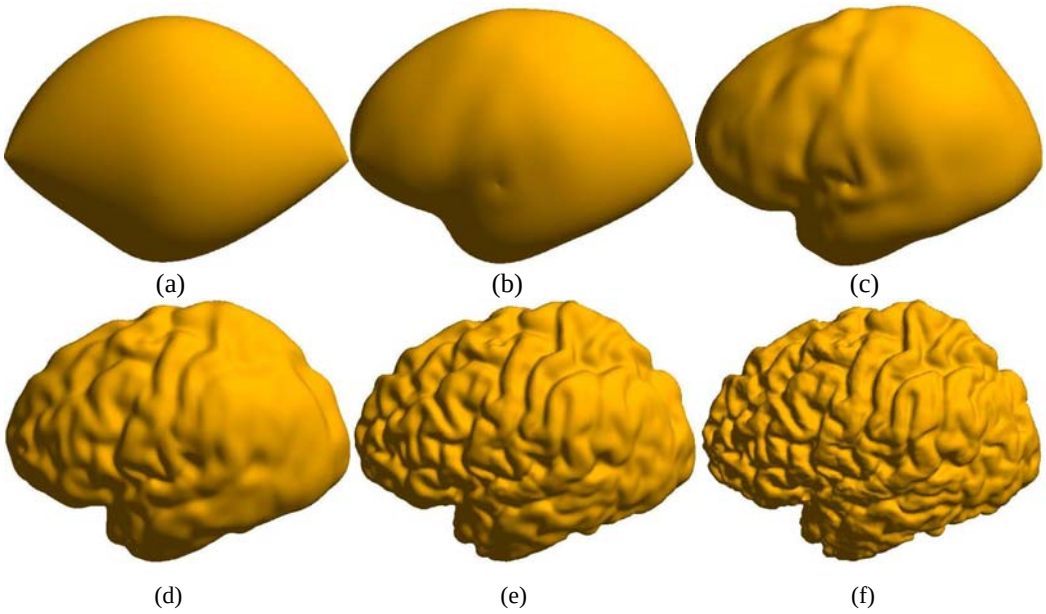

Fig. 5. Figures (a)-(e) present a multiscaled representation of the cortex from courser approximation to finer approximation. Figure (f) is the original cortex.

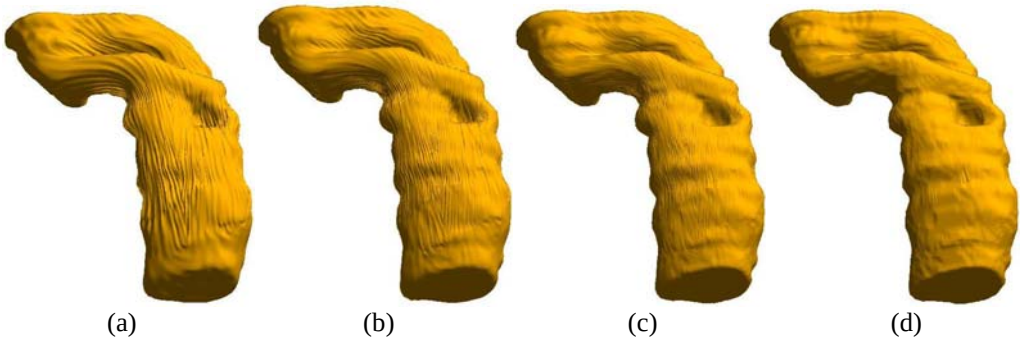

Fig. 6. Figures (a)-(c) are the reconstructed hippocampus using 1000, 2500 and 5000 coefficients, and the relative errors of them from the original shape are 1.171871e-004, 6.172233e-005 and 3.915038e-005 respectively. Figure (d) is the original hippocampus.

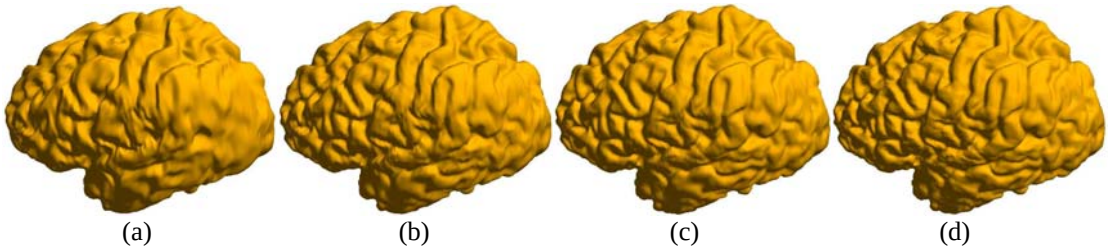

Fig. 7. Figures (a)-(c) are the reconstructed cortices using 1000, 2500 and 5000 coefficients, and the relative errors of them from the original shape are 6.449351e-004, 3.154665e-004 and 1.664914e-004 respectively. Figure (d) is the original cortex.

One advantage of our method over spherical wavelet transform in analyzing biological shapes is that we have a much more flexible choice of wavelets. In particular, we can choose one wavelet with very high vanishing moments so that the representation is very sparse. Figure 8 below shows a comparison of our method to spherical wavelets as used in [9, 10].

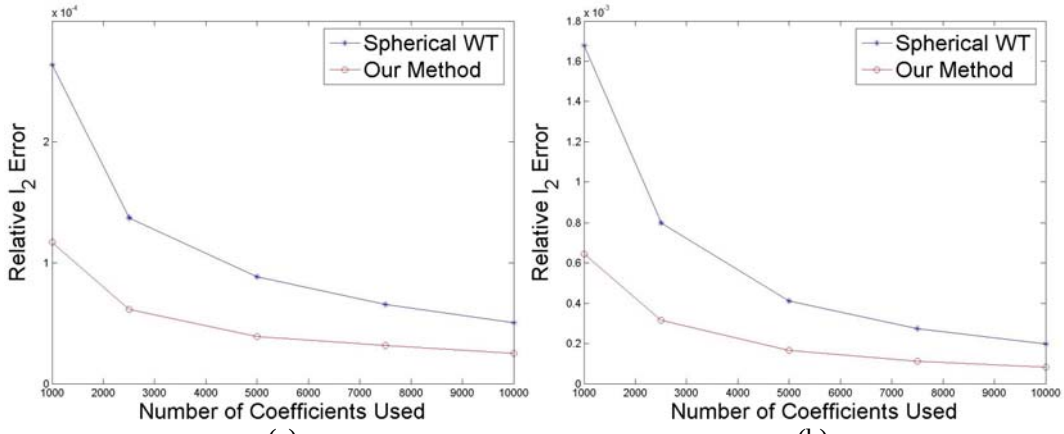

Fig. 8. Figures (a) and (b) are the decay of relative l_2 error verse number of coefficients used, where the underline shapes are the hippocampus and cortex as shown in Figure 6 and 7.

The multiscaled sparse representation provided by the wavelet transform has many applications. For example, one can do shape compression, or in other words, feature dimension reduction for shapes. One can also do shape denoising via thresholding or shrinkage of wavelet coefficients. Since these kinds of applications are not of our main interest, we shall not explore them in further details.

3.2 Non-Parametric Tests

For given two groups of hippocampus, one from healthy population, the other from the one with Alzheimer's disease, we apply Wilcoxon's rank sum test (see e.g. [7]) to the multiscaled curvature-like representation of shapes to find regions on the shape where the two groups are different. The α -value we choose in the results below is 0.05. We note that the tests are more reliable in higher levels than those in lower levels. This is because the shape corresponding to a higher level is a smoothed version of the original shape, which means we have more statistical inference of the object. As one can see from below that the higher the level is, the larger each area of significance will be. In Figure 9 below, we used the mean hippocampus as the reference shape, which is calculated by simply taking an average of all the vector values of hippocampus at every position.

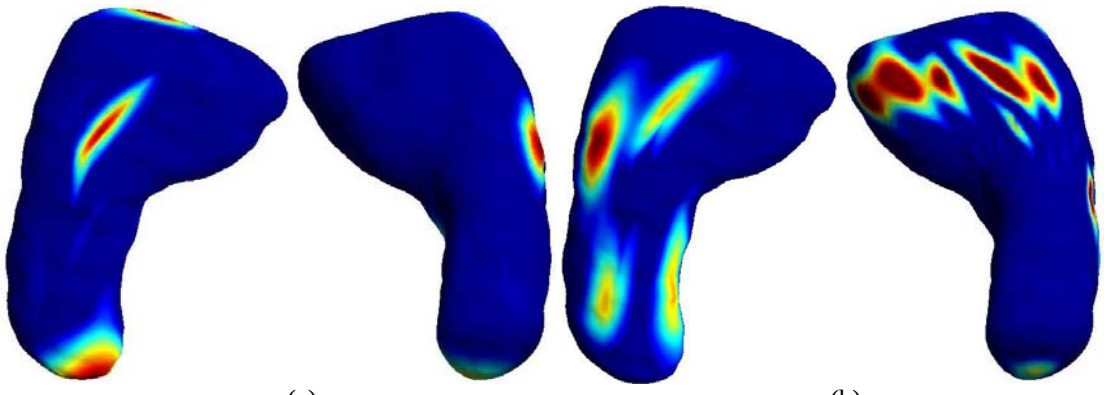

Fig. 9. Figures (a) and (b) show regions of significance of level 5 and 4 respectively. Here, each pair of hippocampus is viewed from the bottom.

4 Discussion

The wavelet-based shape representation technique proposed here allows one to study the geometry, topology and features of general biological shapes using any of the standard wavelet-bases on real-valued Euclidean spaces. The results we obtained are robust and consistent across individuals and populations. In addition to direct representation and shape characterization, this technique allows us to compute mean shapes and improve the shape-analysis statistical power by concentrating the energy of the shape-characteristics in few significant wavelet coefficients, Dinov et. al. [5]. We are in the process of validating the new methodology using larger number of subjects, different types of applications (e.g., studying the population-specific differences in the proportion of gyri to sulcal area) and quantitative comparison with spherical-harmonics, spherical wavelets and tensor-based morphometry techniques.

The computational complexity of the algorithm is $O(N \log N)$ relative to the volume size N. We have a Matlab implementation that we are in the process of converting to stand-alone C++ code, which will be distributed by the end of 2007 on the CCB Software Download pages (http://www.loni.ucla.edu/CCB/Software). We tested the actual computation time of the wavelet decomposition and reconstruction on a PC with Inter(R) Core(TM) 2, 2.13 GHz and 1G physical memory. For a given shape with 65,536 surface points, the computation time is 2-20 seconds, depending on the choice of basis and level of decomposition.

5 Acknowledgement

This work is funded by the National Institutes of Health through the NIH Roadmap for Medical Research, Grant U54 RR021813. Information on the National Centers for Biomedical Computing can be obtained from http://nihroadmap.nih.gov/bioinformatics.

References

1. F. Arandiga, R. Donat and A. Harten: *Multiresolution based on weighted averages of the hat function I: Linear Reconstruction Techniques. UCLA CAM Reports.*, No. 96-25, Aug. 1996.
2. S. Buss and J. Fillmore. *Spherical averages and applications to spherical splines and interpolation*. ACM Transactions on Graphics, 20(2), pp. 95-126, 2001.
3. D. L. Collins, P. Neelin, T. Peters, A. C. Evans, 1994. *Automatic 3D intersubject registration of MR volumetric data in standardized Talairach space*. J. Comput. Assist. Tomogr. 18 (2), 192– 205.
4. I. Daubechies. *Ten Lectures on Wavelets*. CBMS-NSF Lecture Notes nr. 61, SIAM, 1992.
5. I. D. Dinov, J. W. Boscardin, M. S. Mega, E. L. Sowell, A. W. Toga. *A Wavelet-Based Statistical Analysis of fMRI data: I. Motivation and Data Distribution Modeling*, NeuroInformatics, Humana Press, 3(4), 319-343, 2005.
6. A. C. Evans, D. L. Collins, P. Neelin, D. MacDonald, M. Kamber, T. S. Marrett. *Three-dimensional correlative imaging: applications in human brain mapping*. In: Thatcher, R.W., Hallett, M., Zeffiro, T., John, E.R., Huerta, M. (Eds.), Functional Neuroimaging: Technical Foundations. Academic Press, San Diego, pp. 145– 162, 1994.
7. J. D. Gibbons. *Nonparametric Statistical Inference*, 2nd Ed., M. Dekker, 1985.
8. X. Gu, Y. Wang, T. F. Chan, P.M. Thompson and S.-T. Yau. *Genus Zero Surface Conformal Mapping and Its Application to Brain Surface Mapping*. IEEE Transaction on Medical Imaging, 23(8), Aug. 2004, pp. 949-958
   a) <http://www.math.ucla.edu/%7Eylwang/doc/01318721.pdf>.
9. Nain D, Hacker S, Bobick A, Tannenbaum. *A multiscale 3D shape analysis using spherical wavelets*. Proc MICCAI, Oct 26-29 2005; p 459-467.
10. Nain D, Hacker S, Bobick A, Tannenbaum. *A shape-driven 3D segmentation using spherical wavelets*. Proc MICCAI, Oct 2-5, 2006. To Appear.
11. D. MacDonald, A method for identifying geometrically simple surfaces from three dimensional images. PhD thesis, McGill University, 1998.
12. Mazziotta JC, Toga AW, Evans AC, Fox PT, Lancaster J, Zilles K, Woods RP, Paus T, Simpson G, Pike B, Holmes CJ, Collins DL, Thompson PM, MacDonald D, Schormann T, Amunts K, Palomero-Gallagher N, Parsons L, Narr KL, Kabani N (2001) *A probabilistic atlas and reference system for the human brain: International Consortium for Brain Mapping*. Philos Trans R Soc Lond B Biol Sci 356: 1293-1322
13. E. Praun and H. Hoppe, *Spherical parametrization and remeshing*. ACM Trans. Gr. Vol. 22 (3), July 2003.
14. W. Sweldens. *The lifting scheme: A construction of second generation wavelets*. SIAM J. Math. Anal., Vol 29 (2), 511-546, 1997.

15. P. Schröder and W. Sweldens. *Sphereical wavelets: Efficiently representing functions on the sphere*. Computer Graphics Proceedings, (SIGGRAPH 95), Pages 161-172, 1995.
16. D. W. Shattuck, S. R. Sandor-Leahy, K. A. Schaper, D. A. Rottenberg, R. M. Leahy. *Magnetic resonance image tissue classification using a partial volume model.* NeuroImage 13: 856-876, 2001.
17. Y. Shi, P. M. Thompson , G. I. de Zubicaray, S. Rose, Z. Tu, I. Dinov, A. W. Toga, *Direct mapping of hippocampal surfaces with intrinsic shape context*, NeuroImage, 37(3), pp. 792-807, 2007.
18. Y. Shi, P. M. Thompson, I. Dinov, S. Osher, A. W. Toga, *Direct cortical mapping via solving partial differential equations on implicit surfaces*, Medical Image Analysis, 11(3), pp.207-223, 2007
19. J. G. Sled, A. P. Zijdenbos, A. C. Evans, 1998. *A non-parametric method for automatic correction of intensity non-uniformity in MRI data*. IEEE Trans. Med. Imag. 17, 87–97.
20. Paul M. Thompson, Arthur W. Toga. *A Framework for Computational Anatomy.* Springer Berlin / Heidelberg, vol 5, no. 1, 2002.
21. Paul M. Thompson, Agatha D. Lee, Rebecca A. Dutton, Jennifer A. Geaga, Kiralee M. Hayashi, Mark A. Eckert, Ursula Bellugi, Albert M. Galaburda, Julie R. Korenberg, Debra L. Mills, Arthur W. Toga, and Allan L. Reiss. *Abnormal Cortical Complexity and Thickness Profiles Mapped in Williams Syndrome*. The Journal of Neuroscience, vol. 25 no. 16, 2005.
22. Thompson PM, Hayashi KM, de Zubicaray G, Janke AL, Rose SE, Semple J, Herman D, Hong MS, Dittmer S, Doddrell DM, Toga AW. *Dynamics of gray matter loss in Alzheimer's disease*. J Neurosci 23: 994-1005, 2003
23. Paul M. Thompson, Kiralee M. Hayashi, Greig I. de Zubicaray, Andrew L. Janke, Stephen E. Rose, James Semple, Michael S. Hong, David H. Herman, David Gravano, David M. Doddrell and Arthur W. Toga, *Mapping hippocampal and ventricular change in Alzheimer disease*, Neuroimage, vol 22, no. 4, 1754-1766, 2004.
24. Z. Tu, S. Zheng, A. Yuille, A. Reiss, R. Dutton, A.Lee, A.Galaburda, I. Dinov, P. Thompson, A. Toga, *Automated Extraction of the Cortical Sulci Based on a Supervised Learning Approach*, IEEE Tran. on Medical Imaging, vol. 26, no. 4, April, 2007